Electric dipole moments as probes of the $R_{D^{(*)}}$ anomaly

Syuhei Iguro[1,2,3,4,*] and Teppei Kitahara[5,6,2,†]

[1]*Institute for Advanced Research, Nagoya University, Nagoya 464–8601, Japan*
[2]*Kobayashi-Maskawa Institute for the Origin of Particles and the Universe, Nagoya University, Nagoya 464–8602, Japan*
[3]*Institute for Theoretical Particle Physics (TTP), Karlsruhe Institute of Technology (KIT), Wolfgang-Gaede-Str. 1, 76131 Karlsruhe, Germany*
[4]*Institute for Astroparticle Physics (IAP), Karlsruhe Institute of Technology (KIT), Hermann-von-Helmholtz-Platz 1, 76344 Eggenstein-Leopoldshafen, Germany*
[5]*Department of Physics, Graduate School of Science, Chiba University, Chiba 263–8522, Japan*
[6]*CAS Key Laboratory of Theoretical Physics, Institute of Theoretical Physics, Chinese Academy of Sciences, Beijing 100190, China*

(Received 18 April 2024; accepted 17 September 2024; published 11 October 2024)

The measurements of the lepton flavor universality (LFU) in $\mathcal{B}(\bar{B} \to D^{(*)} l \bar{\nu})$ indicate a significant deviation from the standard model prediction at a 3–4σ level, revealing a violation of the LFU ($R_{D^{(*)}}$ anomaly). It is known that the $R_{D^{(*)}}$ anomaly can be easily accommodated by an $SU(2)_L$-singlet vector leptoquark (LQ) coupled primarily to third-generation fermions, whose existence is further motivated by a partial gauge unification. In general, such a LQ naturally leads to additional CP-violating phases in the LQ interactions. In this paper, we point out that the current $R_{D^{(*)}}$ anomaly prefers the CP-violating interaction although $\mathcal{B}(\bar{B} \to D^{(*)} l \bar{\nu})$ are CP-conserving observables. The CP-violating LQ predicts a substantial size of the bottom-quark electric dipole moment (EDM), the chromo-EDM, and also the tau-lepton EDM. Eventually at low energy, the nucleon and electron EDMs are radiatively induced. Therefore, we conclude that the $R_{D^{(*)}}$ anomaly with the $SU(2)_L$-singlet vector LQ provides unique predictions: neutron and proton EDMs with opposite signs and a magnitude of $\mathcal{O}(10^{-27})$ e cm, and suppressed electron EDM. Furthermore, we show that a similar EDM pattern is predicted in an $SU(2)_L$-doublet scalar LQ scenario that can accommodate the $R_{D^{(*)}}$ anomaly as well. These EDM signals could serve as crucial indicators in future experiments.

DOI: 10.1103/PhysRevD.110.075008

I. INTRODUCTION

In the near future, the sensitivities of precision measurements for the elementary particles, particularly the B physics and the electric dipole moments (EDMs), are expected to be improved by an order of magnitude. Many kinds of new physics models will undoubtedly be probed through these improvements.

Currently, a significant deviation from the standard model (SM) prediction has been reported by the *BABAR*, LHCb, Belle, and Belle II experiments [1–15], in measurements of the lepton flavor universality (LFU) in $\bar{B} \to D^{(*)} l \bar{\nu}$. Violation of the LFU is represented by

$$R_{D^{(*)}} \equiv \frac{\mathcal{B}(\bar{B} \to D^{(*)} \tau \bar{\nu}_\tau)}{\mathcal{B}(\bar{B} \to D^{(*)} \ell \bar{\nu}_\ell)}, \tag{1}$$

where ℓ represents an average of the leptons. The up-to-date world average of the data [16,17] is

$$R_D^{\mathrm{exp}} = 0.344 \pm 0.026, \qquad R_{D^*}^{\mathrm{exp}} = 0.285 \pm 0.012, \tag{2}$$

while an up-to-date SM prediction [18–21] is

$$R_D^{\mathrm{SM}} = 0.290 \pm 0.003, \qquad R_{D^*}^{\mathrm{SM}} = 0.248 \pm 0.001, \tag{3}$$

which implies more than 4σ level tension. This $R_{D^{(*)}}$ anomaly naively suggests the existence of $\mathcal{O}(1)$ TeV new physics in the $b \to c \tau \bar{\nu}_\tau$ process, and various kinds of models have been proposed [21,22]. One of new physics candidates is an $SU(2)_L$-singlet vector leptoquark (LQ), dubbed as U_1 LQ whose gauge charge is $(\mathbf{3}, \mathbf{1}, 2/3)$.

*Contact author: igurosyuhei@gmail.com
†Contact author: kitahara@chiba-u.jp

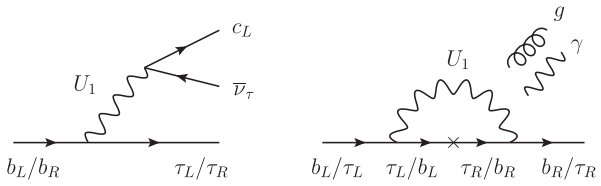

FIG. 1. The vector-LQ (U_1) contributions to $R_{D^{(*)}}$ (left diagram) and the (chromo-) EDMs for the bottom-quark and tau-lepton (right diagram).

The U_1 LQ hypothesis has been widely discussed in connection with a partial gauge unification [23–25] as well as the related flavor processes and the LHC phenomenology have been studied [26,27]. These new physics predictions will be tested in the ongoing Belle II [28] and LHCb experiments [29]. One should note that to avoid the strict constraint from $K_L \to \mu e$ measurements [30,31], (elaborate) $U(2)$ flavor symmetries have been considered for a successful interpretation of the $R_{D^{(*)}}$ anomaly [32–35]. In that case, the U_1 LQ couples primarily to third-generation fermions.

The LQ model naturally brings a CP-violating (CPV) phase coming from the rotation matrices to the mass bases of the left- and right-handed quarks and lepton fields that are not aligned in general. In this paper, it will be clarified that the CPV phase is *necessary* to accommodate the $R_{D^{(*)}}$ anomaly, and this phase also induces the sizable nucleon EDMs at the low energy, which will be testable in the near future (see Fig. 1 for the Feynman diagrams). Although Refs. [36,37] investigated the EDMs in the vector-LQ model in light of the $R_{D^{(*)}}$ anomaly, they focused on the benchmark point parameters and the necessity of the CPV phase was unclear.

Similar to the vector U_1 LQ, an $SU(2)_L$-doublet scalar LQ, R_2, also produces a robust correlation between the $R_{D^{(*)}}$ anomaly and the nucleon EDMs [38–42]. We will also investigate the R_2 LQ scenario in a similar way to the U_1 LQ scenario.

The paper is organized as follows. In Sec. II, we introduce a simplified parametrization of the vector U_1 LQ scenario. In Sec. III, we obtain the formulae for the relevant observables; EDMs, $R_{D^{(*)}}$, and $B_s \to \tau^+\tau^-$ in the U_1 LQ scenario with several comments. In Sec. IV, we summarize the result of the U_1 LQ scenario. Furthermore, in Sec. V, we investigate the scalar R_2 LQ scenario as well. Finally, we conclude in Sec. VI. The additional correlations with the polarization observables are briefly summarized in the Appendix.

II. VECTOR U_1 LQ SCENARIO

In the following Secs. II–IV, we consider a simplified U_1 LQ scenario with a $U(2)$ flavor symmetry. The relevant fermion interactions are described by

$$\mathcal{L} = (\beta_L^{ij}\bar{Q}_i\gamma_\mu P_L L_j + \beta_R^{ij}\bar{d}_i\gamma_\mu P_R e_j)U_1^\mu + \text{H.c.}, \quad (4)$$

with $P_{L/R} = (1 \mp \gamma_5)/2$ in the fermion mass eigenbasis. Although additional vectorlike fermions are needed in Eq. (4) to obtain the ideal flavor structure in the UV complete model [43], we focus on the 3×3 flavor structures. This simplification is valid to consider the EDMs, and we will discuss this point in Sec. III D. This class of UV complete model is called 4321 gauge-group model [23,44].

We consider the following flavor texture [25,43]:

$$\beta_L^{ij} \simeq \beta_L^{33}\begin{pmatrix} 0 & 0 & -c_d s_{q_2} s_\chi \left|\frac{V_{td}}{V_{ts}}\right| \\ 0 & 0 & c_d s_{q_2} s_\chi \\ 0 & 0 & c_\chi \end{pmatrix},$$
$$\beta_R^{ij} \simeq \beta_L^{33} e^{i\phi_R}\begin{pmatrix} 0 & 0 & 0 \\ 0 & 0 & 0 \\ 0 & 0 & 1 \end{pmatrix}, \quad (5)$$

where $c_d \simeq 0.98$, corresponding to a case of $s_{l_2} \simeq s_\tau \simeq 0$ in the literature. Here, s_i and c_i represent flavor rotations $\sin\theta_i$ and $\cos\theta_i$ to bring the SM fermions to their mass eigenbasis. Note that $|\beta_L^{33}| \simeq |\beta_R^{33}|$ results from the gauge symmetry in the UV complete model. In this setup, ϕ_R is an arbitrary CPV phase; the other CPV phases can be absorbed by a redefinition of ϕ_R [45]. Therefore, the relative phase between β_L and β_R interactions plays an important role in the CPV observables. In our analysis, only three parameters are relevant to the phenomenology: β_L^{33}/m_{U_1}, $\beta_L^{23}/\beta_L^{33}(= c_d s_{q_2} s_\chi/c_\chi)$, and the CPV angle ϕ_R.

III. EDMS AND OTHER OBSERVABLES

In this section, we concisely summarize the phenomenological effects of the U_1 LQ.

First, we focus on the LQ contributions to EDMs. The effective Lagrangian for the EDM (d_f) and chromo-EDM interactions ($\tilde{d}_f$) are expressed as

$$\mathcal{L}_{\text{eff}} = -\frac{i}{2}\sum_f (d_f \bar{f}\sigma_{\mu\nu}\gamma_5 f F^{\mu\nu} + g_s \tilde{d}_f \bar{f}\sigma_{\mu\nu} T^a \gamma_5 f G^a_{\mu\nu}), \quad (6)$$

with $\sigma_{\mu\nu} = \frac{i}{2}[\gamma_\mu, \gamma_\nu]$. Based on Refs. [37,46,47], the U_1 LQ contributions to the tau-lepton and bottom-quark (chromo-) EDMs are (see Fig. 1 right diagram)

$$d_\tau = -\frac{3e}{8\pi^2}\frac{m_b(\Lambda_{\text{LQ}})}{m_{U_1}^2}\text{Im}[\beta_L^{33}(\beta_R^{33})^*], \quad (7)$$

$$d_b(\Lambda_{\text{LQ}}) = -\frac{5e}{24\pi^2}\frac{m_\tau}{m_{U_1}^2}\text{Im}[\beta_L^{33}(\beta_R^{33})^*], \quad (8)$$

$$\tilde{d}_b(\Lambda_{\rm LQ}) = -\frac{1}{8\pi^2}\frac{m_\tau}{m_{U_1}^2}{\rm Im}[\beta_L^{33}(\beta_R^{33})^*], \tag{9}$$

and there is no contribution to the other EDMs at the LQ mass scale, $\mu = \Lambda_{\rm LQ}$. Note that the Weinberg operator would be induced at two-loop level, but it is suppressed by $m_b m_\tau / m_{U_1}^4$, and we discarded it [38]. While the QCD renormalization-group (RG) evolution does not affect d_τ, we have incorporated the RG evolutions from $\Lambda_{\rm LQ}$ to $\mu_b (= m_b)$, which is known to relax the EDM bound [48]. Including the first nontrivial photon-loop effect [39,49], for $\Lambda_{\rm LQ} = 2$ TeV, we obtain [50–52]

$$d_b(\mu_b) = 0.82 d_b(\Lambda_{\rm LQ}) + 0.21 e\tilde{d}_b(\Lambda_{\rm LQ}), \tag{10}$$

$$\tilde{d}_b(\mu_b) = 0.08\frac{d_b(\Lambda_{\rm LQ})}{e} + 0.90\tilde{d}_b(\Lambda_{\rm LQ}). \tag{11}$$

After integrating out the tau and bottom quark at low energy, the electron EDM is induced by the tau and bottom-quark EDMs from QED three-loop radiative corrections [53]. Furthermore, a semileptonic CP-odd operator, $(\bar{e}i\gamma_5 e)(\bar{p}p + \bar{n}n)$, is also induced from QED two-loop diagrams [54,55], which eventually mimics the electron EDM (called an equivalent electron EDM) in the experiments [56,57]. By using a result of the improved analysis for the three-loop calculation [58], we obtain

$$\begin{aligned} d_e^{\rm equiv} = {} & [4.7\times 10^{-13} + 8.8(1\pm 0.1)\times 10^{-12}] d_b(\mu_b) \\ & + (9.9\times 10^{-12} + 9.2\times 10^{-14}) d_\tau. \end{aligned} \tag{12}$$

Here, the first terms in each parenthesis come from the QED three-loop contribution, while the second terms come from the semileptonic CP-odd operator [55]. Note that the latter calculation is a result in the case of the HfF^+ molecule system [59] (see Refs. [56,57] for the other molecules). The dominant theoretical uncertainty comes from the semileptonic CP-odd operator induced by the bottom-quark EDM, which is estimated as 10% [55].

By a similar but more involved processes, the nucleon (neutron and proton) EDMs are induced from the bottom-quark EDM and chromo-EDM. Short-distance contributions come from the light-quark EDM and chromo-EDMs, $d_N^{\rm light}$, and the Weinberg operator, $d_N^{\rm W}$ [60–62], while a long-distance contribution arises from a CP-odd photon-gluon operator ($GGG\tilde{F}$), $d_N^{\tilde{F}G^3}$ [55]. For the neutron and proton EDMs, we numerically obtain

$$d_N = d_N^{\rm light} + d_N^{\rm W} + d_N^{\tilde{F}G^3} \quad ({\rm for}\ N = n, p), \tag{13}$$

with

$$d_n^{\rm light} = 4.0\times 10^{-7} e\tilde{d}_b(\mu_b) + 4.0\times 10^{-8} d_b(\mu_b), \tag{14}$$

TABLE I. The current 90% confidence level (CL) upper limits and future prospects for electron, neutron, and proton EDMs.

EDM [e cm]	90% CL limit	Future sensitivity
$\lvert d_e\rvert$	$\leq 4.1\times 10^{-30}$ [59]	$\mathcal{O}(10^{-31})$ [78]
$\lvert d_n\rvert$	$\leq 1.8\times 10^{-26}$ [79]	$\mathcal{O}(10^{-27})$ [80–83]
		$\mathcal{O}(10^{-28})$ [84]
$\lvert d_p\rvert$	$\leq 2.1\times 10^{-25}$ [85]	$\mathcal{O}(10^{-29})$ [86,87]

$$d_p^{\rm light} = -3.3\times 10^{-7} e\tilde{d}_b(\mu_b) + 9.1\times 10^{-9} d_b(\mu_b), \tag{15}$$

$$d_n^{\rm W} = -5.4(1\pm 0.5)\times 10^{-5} e\tilde{d}_b(\mu_b), \tag{16}$$

$$d_p^{\rm W} = 7.7(1\pm 0.5)\times 10^{-5} e\tilde{d}_b(\mu_b), \tag{17}$$

$$d_N^{\tilde{F}G^3} \approx 7\times 10^{-7} d_b(\mu_b) \quad ({\rm for}\ N = n, p). \tag{18}$$

For $d_N^{\rm light}$, the QCD sum-rule estimate is used [57,63–66] (where the Peccei-Quinn mechanism is assumed to suppress the $\bar{\theta}$ parameter), whose overall normalization is determined by the lattice result [67]. The light-quark EDMs are induced by the bottom-quark EDM [55] and chromo-EDM [58], while the light-quark chromo-EDMs are induced from the bottom-quark chromo-EDM [52]. For $d_N^{\rm W}$, the QCD sum-rule estimates [57,68,69] (see also [70]) are used. Note that although all the above terms have 10%–30% theoretical uncertainties, we suppressed them except for the leading one ($d_N^{\rm W}$). For $d_N^{\tilde{F}G^3}$, the QCD sum-rule technique is also used and the numerics should be understood as an order-of-magnitude estimation [55].

It is found that the overwhelmingly dominant contribution to the nucleon EDMs comes from the Weinberg operator. Also, the theoretical uncertainty is dominated by the Weinberg operator, which is estimated as 50% [69]. Although the accuracy of the lattice calculations is currently not competitive [71–77], they will provide complementary inputs in the future. We emphasize that the predicted neutron and proton EDMs must be the same size with opposite signs [69].

The current upper bounds and the future prospects for the electron, neutron, and proton EDMs are summarized in Table I.

A. $R_{D^{(*)}}$

The U_1 LQ can naturally explain the $R_{D^{(*)}}$ anomalies. After integrating out the LQ and the weak bosons, the effective Lagrangian is given by

$$\mathcal{L}_{\rm eff} = -2\sqrt{2} G_F V_{cb}[(1 + C_{V_L}) O_{V_L} + C_{S_R} O_{S_R}], \tag{19}$$

with $O_{V_L} = (\bar{c}\gamma^\mu P_L b)(\bar{\tau}\gamma_\mu P_L \nu_\tau)$, $O_{S_R} = (\bar{c} P_R b)(\bar{\tau} P_L \nu_\tau)$, and the Wilson coefficients (WCs) at $\mu = \mu_b$ are

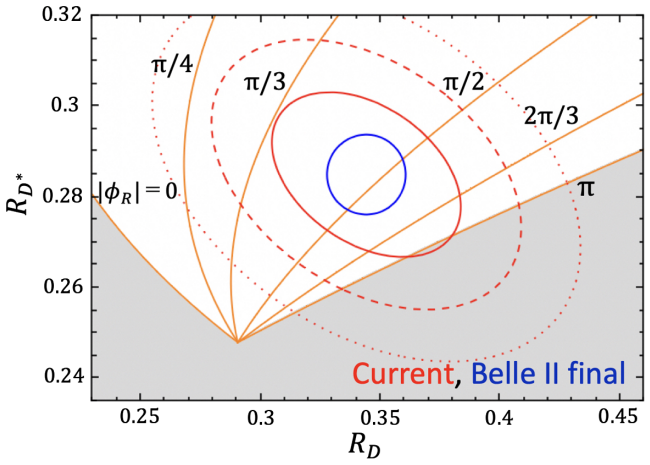

FIG. 2. The orange contour represents the CPV phase $|\phi_R|$ on the plane of R_D–R_{D^*} in the simplified U_1 scenario. The red solid, dashed, and dotted contours correspond to $1, 2, 3\sigma$ of the experimental world average [17]. The blue circle denotes a sensitivity projection of the Belle II experiment [28] assuming the current central values. The gray-shaded region is out of the model prediction.

$$C_{V_L}(\mu_b) = \frac{\eta_{V_L}}{2\sqrt{2}G_F V_{cb}} \frac{\beta_L^{23}(\beta_L^{33})^*}{m_{U_1}^2}, \tag{20}$$

$$C_{S_R}(\mu_b) = -\frac{\eta_{S_R}}{\sqrt{2}G_F V_{cb}} \frac{\beta_L^{23}(\beta_R^{33})^*}{m_{U_1}^2}, \tag{21}$$

where η_{V_L} and η_{S_R} are coefficients of the QCD corrections [88–90]. For $\Lambda_{\rm LQ} \simeq 2$–$4$ TeV, $\eta_{V_L} \simeq 1.1$ and $\eta_{S_R} \simeq 2.0$ [21]. Furthermore, assuming the simplified flavor texture in Eq. (5), these two WCs can be correlated with being

$$C_{S_R}(\mu_b) \simeq -3.6 e^{-i\phi_R} C_{V_L}(\mu_b). \tag{22}$$

By using the numerical formulas for $R_{D^{(*)}}$ in Ref. [21], based on the heavy quark effective theory form factors [19], we show a correlation between $R_{D^{(*)}}$ and the CPV phase ϕ_R in Fig. 2. Since $R_{D^{(*)}}$ are the CP-conserving observables, they depend on only $\cos\phi_R$ and are invariant under $\phi_R \leftrightarrow -\phi_R$. The orange contour denotes the values of $|\phi_R|$ with varying β_L^{33}/m_{U_1}. We use $\beta_L^{23}/\beta_L^{33} = \lambda \simeq 0.225$ as a typical reference value [43]. The gray-shaded region cannot be predicted within the simplified U_1 LQ model. It is found that large ϕ_R ($\pi/3 < |\phi_R|$) is favored to accommodate the $R_{D^{(*)}}$ anomaly, while a CP-conserving scenario of $\phi_R = 0$ can be excluded by the current data. One should note that the U_1 LQ model also leads to deviations from the SM predictions in other $b \to c\tau\bar{\nu}$ observables, τ polarization asymmetry and the LFU violation in $\Lambda_b \to \Lambda_c l\bar{\nu}$, which will be shown in the Appendix.

B. $B_s \to \tau^+\tau^-$

Within the SM, $B_s \to \tau^+\tau^-$ is suppressed by the one-loop factor and also the chirality factor, $m_\tau^2/m_{B_s}^2$. On the other hand, the U_1 LQ contributions are induced at the tree level and further the chirality suppression can be avoided. Therefore, $B_s \to \tau^+\tau^-$ is significantly affected by the LQ. Currently, the LHCb with run 1 data sets the upper limit on the branching ratio at 95% CL as [91]

$$\mathcal{B}(B_s \to \tau^+\tau^-) \le 6.8 \times 10^{-3}. \tag{23}$$

The future prospect of the LHCb run 3 has been estimated to improve the sensitivity by a factor of 5 [92]. The U_1 LQ contribution to $B_s \to \tau^+\tau^-$ including the QCD corrections is given by [43]

$$\begin{aligned}\frac{\mathcal{B}(B_s \to \tau^+\tau^-)}{\mathcal{B}(B_s \to \tau^+\tau^-)^{\rm SM}} &\simeq \left|1 + \frac{\pi}{\sqrt{2}\alpha G_F V_{tb}V_{ts}^* m_{U_1}^2} \beta_L^{23}(-0.26\beta_L^{33} + 1.8\beta_R^{33})^*\right|^2 \\ &+ \left(1 - \frac{4m_\tau^2}{m_{B_s}^2}\right)\left|\frac{1.8\pi}{\sqrt{2}\alpha G_F V_{tb}V_{ts}^* m_{U_1}^2} \beta_L^{23}(\beta_R^{33})^*\right|^2. \end{aligned} \tag{24}$$

It is noted that the effect from the CPV phase ϕ_R is mild due to the smallness of the SM contribution.

C. LHC high-p_T bound

We employed a public tool `HighPT` [93] to derive the collider constraint from $pp \to \tau^+\tau^-$ and $pp \to \tau\nu$ data. Currently, the dominant constraint comes from the high-p_T di-τ search from the ATLAS Collaboration [94] (see also Refs. [44,95] for the relevant study). At the CMS, an excess has been found in the high-p_T tail region [96,97]. However, the ATLAS does not find excess in the region.[1] On the other hand, the constraint from high-p_T mono-τ search is currently less constraining [99,100]. However, it has been pointed out that requiring an additional b-tagged jet can improve the sensitivity so that this channel is competitive with the di-τ channel [101,102].

D. Comment on other constraints

It is known that although loop-induced LQ contributions to $B_s - \bar{B}_s$ mixing give a severe constraint, once additional vectorlike fermions are introduced in the UV complete model, the constraint can be naturally avoided thanks to the GIM-like mechanism [26,43,103–107]. We emphasize that the vectorlike fermions do not mix the SM right-handed fermions in the UV complete model, and the EDMs are not

[1]More detailed experimental comparisons and/or statistics are necessary to conclude the difference between the CMS and ATLAS results [98].

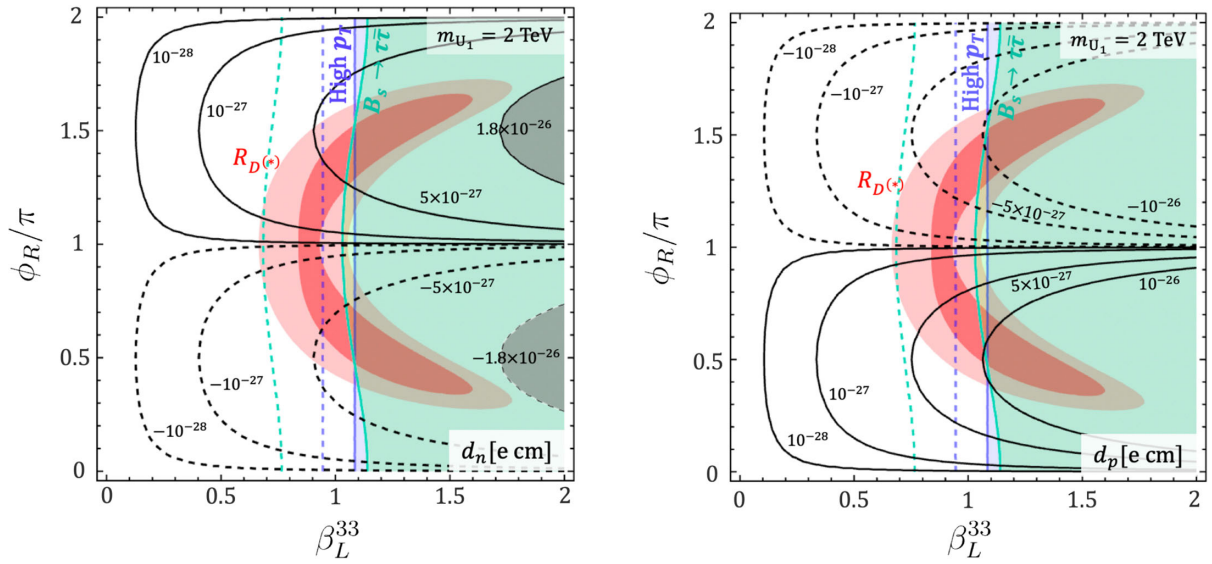

FIG. 3. The predicted neutron and proton EDMs are shown by the black contours in the left and right panels, respectively, where the solid (dashed) lines represent positive (negative) EDMs, in the U_1 scenario. The gray-shaded region is excluded by the current upper bound on the neutron EDM [79]. The red (light red) region can explain the $R_{D^{(*)}}$ anomaly at 1σ (2σ) level. The blue and green regions are excluded by the high-p_T bound and $B_s \to \tau^+\tau^-$, respectively. The estimated sensitivities based on upcoming run 3 data are shown by the dashed blue and green lines. We set $m_{U_1} = 2$ TeV and $\beta_L^{23}/\beta_L^{33} = \lambda$.

induced from the vectorlike fermion loops [43]. Therefore, the EDMs provide a unique prediction of the model.

The similar sensitivity to $B_s \to \tau^+\tau^-$ could be obtained from the measurement of $B \to K\tau^+\tau^-$ at the Belle II [27], while we omitted it since the current bound is much weaker. Although $B^- \to \tau\bar{\nu}$ is also modified in the simplified flavor texture, a moderate β_L^{13} suppresses the constraint [43].

Additionally, we would like to comment on the possibility of further contributions to the EDMs from other scalar particles, which are required for the gauge symmetry breaking. In the 4321 model, in addition to the U_1 LQ, the R_2 scalar LQ is also introduced (it is called H_{15} field in Ref. [43]). This R_2 LQ could produce two large EDMs: (1) top-quark and (2) tau-lepton EDMs. We estimated both contributions and found that (1) predicted top-quark EDM is 2 orders of magnitude smaller than the current experimental bound $|d_t| < 5 \times 10^{-20}\ e\,\mathrm{cm}$ [108], and (2) the predicted tau-lepton EDM is 2 orders of magnitude larger by a factor of m_t/m_c than Eq. (31). The latter induces the electron EDM at $\mathcal{O}(10^{-30})\ e\,\mathrm{cm}$, which can be probed by future experiments; see Table I. Note that this R_2 LQ in the 4321 model can not account for the $R_{D^{(*)}}$ anomaly.

IV. RESULT OF THE U_1 LQ SCENARIO

In Figs. 3 and 4, we show the correlations between the predicted nucleon (neutron and proton) EDMs and the $R_{D^{(*)}}$ anomaly in the U_1 LQ model. Here, $m_{U_1} = 2$ TeV and $\beta_L^{23}/\beta_L^{33} = \lambda$ are taken as reference values. Black contours in Fig. 3 indicate the neutron and proton EDMs in the left and right panels, respectively, where the solid (dashed) lines represent positive (negative) EDMs. We used the central values of Eqs. (16) and (17) for the estimates of the nucleon EDMs. The blue and green regions are excluded by the high-p_T bound and $B_s \to \tau^+\tau^-$, respectively. The estimated sensitivities based on upcoming tun 3 data are shown by the dashed blue and green lines in Fig. 3. It is noted that $B_s \to \tau^+\tau^-$ at run 3 will be able to cover most of the preferred parameter region at the 2σ level. We also show the correlations on the R_D–R_{D^*} plane in Fig. 4.

These figures show that some of the preferred areas are already excluded by both the high-p_T bound and $B_s \to \tau^+\tau^-$. In the allowed regions, the predicted magnitudes of the nucleon EDMs are $|d_n| < 7 \times 10^{-27}\ e\,\mathrm{cm}$ and $|d_p| < 1 \times 10^{-26}\ e\,\mathrm{cm}$. Very excitingly, in the near future, several experiments will probe the neutron EDM at $\mathcal{O}(10^{-27})\ e\,\mathrm{cm}$ precision [80–83], and eventually, $\mathcal{O}(10^{-28})\ e\,\mathrm{cm}$ [84]. Furthermore, two experiments are proposed that the proton EDM will be proved at $\mathcal{O}(10^{-29})\ e\,\mathrm{cm}$ precision [86,87]. Therefore, we conclude that nucleon EDMs with their opposite signs and $B_s \to \tau^+\tau^-$ will be a smoking-gun signal of the U_1 LQ model.

On the other hand, the induced electron EDM from Eq. (12) is $|d_e| < 10^{-32}\ e\,\mathrm{cm}$, which is a few orders away from the future prospect, but the suppressed electron EDM is also a unique prediction of this model.

V. SCALAR R_2 LQ SCENARIO

In this section, we perform the same analysis as the main text for the R_2 LQ scenario. The gauge charge of the scalar LQ R_2 is $(\mathbf{3}, \mathbf{2}, 7/6)$ and the $SU(2)_L$-doublet $(R_2^{\frac{5}{3}}, R_2^{\frac{2}{3}})$ has a

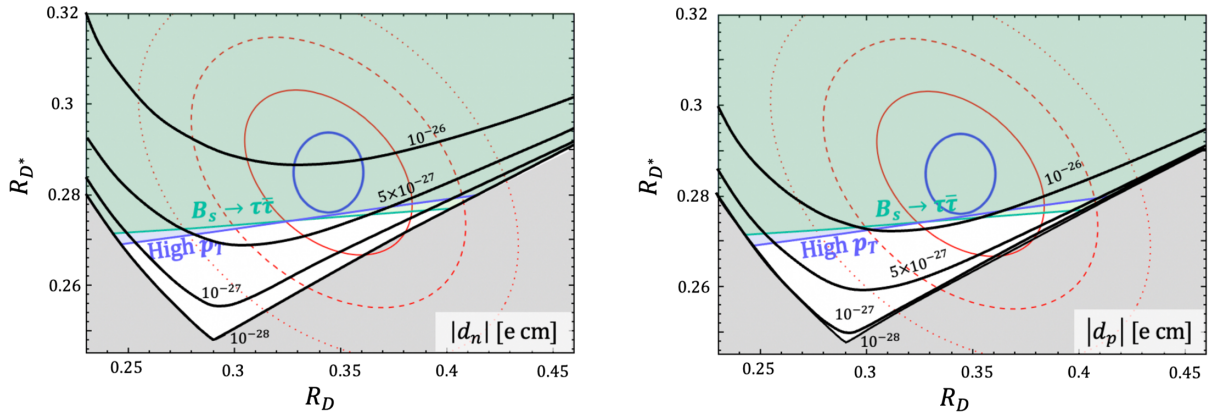

FIG. 4. The absolute values of the predicted neutron and proton EDMs are shown by the black contours in the left and right panels, respectively, in the U_1 scenario. Constraints from the high-p_T search and $B_s \to \tau^+\tau^-$ are represented by the blue and green regions, respectively. The gray-shaded regions are out of the model prediction. We set $m_{U_1} = 2$ TeV and $\beta_L^{23}/\beta_L^{33} = \lambda$.

common mass m_{R_2}. The fermion interactions are described by

$$\mathcal{L} = -y_L^{ij}\bar{u}_i R_2^T \epsilon P_L L_j + y_R^{ij}\bar{Q}_i R_2 P_R e_j + \text{H.c.}, \quad (25)$$

with $\epsilon_{12} = 1$.

The tree-level $R_2^{\frac{2}{3}}$ exchange contributes to the $b \to c\tau\bar{\nu}_\tau$ process with the WCs of [21]

$$C_{S_L}(\Lambda_{\rm LQ}) = 4C_T(\Lambda_{\rm LQ}) = \frac{1}{4\sqrt{2}G_F V_{cb}}\frac{y_L^{23}(y_R^{33})^*}{m_{R_2}^2}, \quad (26)$$

where the normalization of the effective Lagrangian is the same as that in the main text with

$$O_{S_L} = (\bar{c}P_L b)(\bar{\tau}P_L\nu_\tau), \quad (27)$$

$$O_T = (\bar{c}\sigma^{\mu\nu}P_L b)(\bar{\tau}\sigma_{\mu\nu}P_L\nu_\tau). \quad (28)$$

Through the RG evolution, the WCs at the low energy are obtained as [21]

$$C_{S_L}(\mu_b) = 1.91C_{S_L}(\Lambda_{\rm LQ}) - 0.38C_T(\Lambda_{\rm LQ}), \quad (29)$$

$$C_T(\mu_b) = 0.89C_T(\Lambda_{\rm LQ}), \quad (30)$$

for $\Lambda_{\rm LQ} \simeq 2$ TeV.

Next, we consider the EDM part. Although the $R_2^{\frac{2}{3}}$ component does not contribute to any EDMs, it is known that the $R_2^{\frac{5}{3}}$ LQ affects the tau-lepton and charm-quark (chromo-) EDMs [38,40,109],

$$d_\tau = -\frac{e}{32\pi^2}\frac{m_c(\Lambda_{\rm LQ})}{m_{R_2}^2}\text{Im}[y_L^{23}V_{cb}^*(y_R^{33})^*] \times\left(1 + 4\ln\frac{m_c^2}{m_{R_2}^2}\right), \quad (31)$$

$$d_c(\Lambda_{\rm LQ}) = \frac{e}{32\pi^2}\frac{m_\tau}{m_{R_2}^2}\text{Im}[y_L^{23}V_{cb}^*(y_R^{33})^*] \times\left(\frac{4}{3} + 2\ln\frac{m_\tau^2}{m_{R_2}^2}\right), \quad (32)$$

$$\tilde{d}_c(\Lambda_{\rm LQ}) = \frac{1}{32\pi^2}\frac{m_\tau}{m_{R_2}^2}\text{Im}[y_L^{23}V_{cb}^*(y_R^{33})^*]. \quad (33)$$

Note that unlike the vector U_1 LQ scenario, the EDMs receive large logarithmic corrections. They are interpreted as the operator mixing between the scalar-type semileptonic operator and dipole operator in the RG evolution [38,110]. At the low energy $\mu_c(= m_c)$, the charm-quark (chromo-) EDMs receive the following RG effects, including the first nontrivial QED effect,

$$d_c(\mu_c) = 0.76d_c(\Lambda_{\rm LQ}) - 0.58e\,\tilde{d}_c(\Lambda_{\rm LQ}), \quad (34)$$

$$\tilde{d}_c(\mu_c) = -0.05\frac{d_c(\Lambda_{\rm LQ})}{e} + 0.87\,\tilde{d}_c(\Lambda_{\rm LQ}), \quad (35)$$

with $\Lambda_{\rm LQ} = 2$ TeV.

After integrating out the tau and the charm quark, the equivalent electron EDM is induced as

$$d_e^{\rm equiv} = [-1.2\times10^{-11} - 5.4(1\pm0.1)\times10^{-10}]d_c(\mu_c) + (9.9\times10^{-12} + 9.2\times10^{-14})d_\tau. \quad (36)$$

Similar to the U_1 LQ case, the nucleon EDMs $d_N = d_N^{\rm light} + d_N^{\rm W} + d_N^{\tilde{F}G^3}$ for $N = n, p$ are radiatively induced as

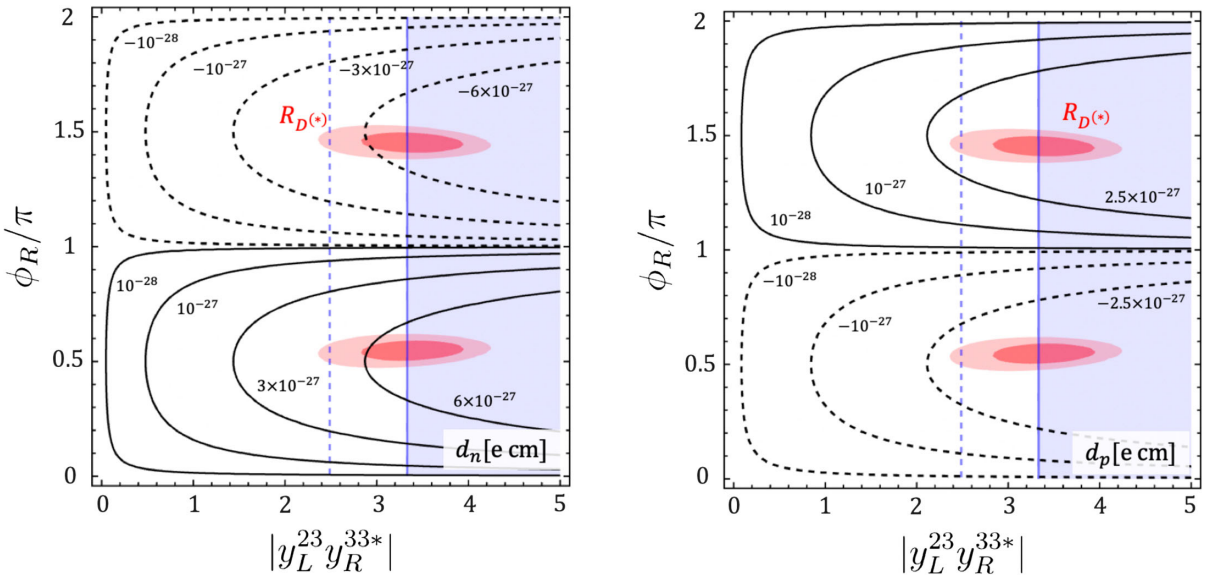

FIG. 5. The predicted neutron and proton EDMs are shown in the R_2 scenario. The red (light red) region can explain the $R_{D^{(*)}}$ anomaly at 1σ (2σ) level. The blue and green regions are excluded by the high-p_T bound. The estimated sensitivities based on upcoming run 3 data are shown by the dashed blue lines. We set $m_{R_2} = 2$ TeV and $|y_L^{23}|/|y_R^{33}| = 0.7$.

$$d_n^{\rm light} = -2.0 \times 10^{-6} e\tilde{d}_c(\mu_c) + 9.2 \times 10^{-7} d_c(\mu_c), \quad (37)$$

$$d_p^{\rm light} = -4.8 \times 10^{-7} e\tilde{d}_c(\mu_c) + 2.2 \times 10^{-7} d_c(\mu_c), \quad (38)$$

$$d_n^{\rm W} = -5.5(1 \pm 0.5) \times 10^{-4} e\tilde{d}_c(\mu_c), \quad (39)$$

$$d_p^{\rm W} = 7.9(1 \pm 0.5) \times 10^{-4} e\tilde{d}_c(\mu_c), \quad (40)$$

$$d_N^{\tilde{F}G^3} \approx 3 \times 10^{-5} d_c(\mu_c) \quad (\text{for } N = n, p). \quad (41)$$

It must be emphasized that the charm quark should not be integrated out for the nucleon EDM evaluations if possible, because charm-quark mass is close to the hadronic scale. It is known that one can investigate the nonperturbative QCD contribution from the charm-quark EDM by using the charm tensor charge g_T^c with $d_N \supset g_T^c d_c$. The latest lattice result is $g_T^c = (-2.4 \pm 1.6) \times 10^{-4}$, where the matching scale is $\mu = 2$ GeV [67]. This has still large uncertainty. Furthermore, the value is an order of magnitude larger than the QCD sum-rule result [55] [$d_N^{\tilde{F}G^3}$ in Eq. (41)] with opposite sign. Therefore, we investigate two different evaluations: $d_N = d_N^{\rm light} + d_N^{\rm W} + d_N^{\tilde{F}G^3}$ and $d_N = g_T^c d_c$. References [39,40] investigated the former contribution, while Refs. [38,41,42] did the latter one, and none of the literature compares these two contributions.

Similar to the U_1 LQ case, only a single CPV phase, the relative phase between y_L^{23} and y_R^{33}, is relevant. In this section, we set $y_L^{23} = |y_L^{23}|$ and $y_R^{33} = |y_R^{33}| \exp(i\phi_R)$. Then, the free parameters are only three: $|y_R^{33}|/m_{R_2}$, $|y_L^{23}|/|y_R^{33}|$, and the CPV angle ϕ_R.

We also evaluate the high-p_T bound by using `HighPT`. Note that both components $(R_2^{\frac{5}{3}}, R_2^{\frac{2}{3}})$ contribute to the bound.

In Figs. 5 and 6, we show the correlations between the nucleon EDMs and the $R_{D^{(*)}}$ anomaly in the R_2 LQ model parameter space and the R_D–R_{D^*} plane, respectively. In both plots, we take $m_{R_2} = 2$ TeV and $|y_L^{23}|/|y_R^{33}| = 0.7$. The blue shaded regions are excluded by the high-p_T analysis. We found that the value $|y_L^{23}|/|y_R^{33}| \approx 0.7$ can alleviate this bound, and taking $|y_L^{23}|/|y_R^{33}| \gg 0.7$ and $\ll 0.7$ are incompatible to the $R_{D^{(*)}}$ anomaly at the 1σ level. In Fig. 5, the dashed blue lines represent the estimated run 3 sensitivity of the high-p_T search. We also show the CPV phase $|\phi_R|$ by the orange contour in Fig. 6. It is clearly shown that the $R_{D^{(*)}}$ anomaly predicts the large CPV phase ϕ_R. In both figures, we show the neutron and proton EDMs calculated by $d_N = d_N^{\rm light} + d_N^{\rm W} + d_N^{\tilde{F}G^3}$. In the allowed regions, the predicted magnitudes of the nucleon EDMs are $|d_n| < 7 \times 10^{-27}$ e cm and $|d_p| < 4 \times 10^{-27}$ e cm. It is worth noting that the EDM predictions in Fig. 6 are insensitive to the ratio of $|y_L^{23}|/|y_R^{33}|$.

On the other hand, in Fig. 7, we plot the nucleon EDM calculated by the charm tensor charge $d_N = g_T^c d_c$. We found that this evaluation is a factor of 3 to 5 larger than Fig. 6. Also, the $R_{D^{(*)}}$ preferred region is mostly excluded by the current upper bound on d_n [79]. Note that both estimations ($d_N^{\rm W}$ and $g_T^c d_c$) contain $\mathcal{O}(50)\%$ theoretical uncertainties, which are not included in our analysis. Nevertheless, we conclude that the predicted nucleon EDMs are large enough to be observed in the next generation experiments.

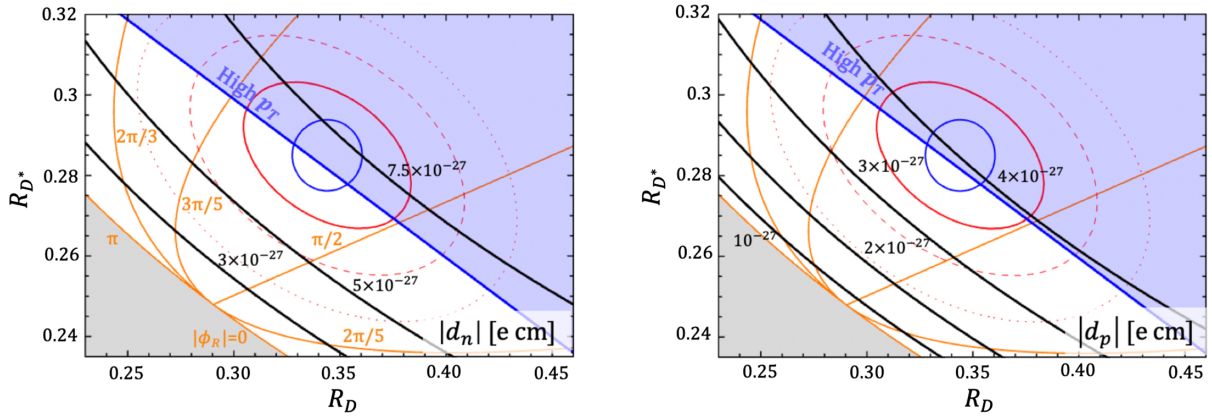

FIG. 6. The absolute values of the predicted neutron and proton EDMs are shown by the black contours in the left and right panels, respectively, in the R_2 scenario. The orange contour represents the CPV phase $|\phi_R|$. The blue regions are excluded by the high-p_T bound. We set $m_{R_2} = 2$ TeV and $|y_L^{23}|/|y_R^{33}| = 0.7$.

Note that there is no R_2 LQ contributions to $B_s \to \tau^+\tau^-$, unlike the U_1 LQ scenario. On the other hand, the R_2 LQ contributes to $Z \to \tau^+\tau^-$ at the one-loop level [111,112], which has a comparable sensitivity with the high-p_T bound [42].

Moreover, we found that the induced electron EDM is $|d_e| < 4 \times 10^{-32}$ e cm, and it is difficult to probe it by the proposed future experiments.

For the completeness, we show τ polarization asymmetry and the LFU violation in $\Lambda_b \to \Lambda_c l\bar{\nu}$ in the Appendix.

VI. SUMMARY AND DISCUSSION

In this paper, we established a robust bridge between the electric dipole moments and the flavor anomaly in $\bar{B} \to D^{(*)} l\bar{\nu}$ through the $SU(2)_L$-singlet vector LQ coupled primarily to third-generation fermions as well as the $SU(2)_L$-doublet scalar LQ scenarios. In these LQ interactions, there is one CP-violating phase required to accommodate the $R_{D^{(*)}}$ anomaly, and hence, CP-violating phenomena are inevitably predicted. We investigated various EDMs and found that neutron and proton EDMs are induced with opposite signs, and predicted magnitudes are well within the reach of the sensitivities of future experiments. It is also found that in the U_1 LQ scenario $B_s \to \tau^+\tau^-$ at LHCb run 3 will become another smoking-gun signal, while it is absent in the R_2 LQ scenario.

Correlations with other CP V phenomena, *e.g.*, $\Delta A_{CP}(B \to X_s\gamma)$, will also be interesting, and we leave them as a future work. It is known that the remaining discrepancies in $b \to s\ell^+\ell^-$ could also be solved by the U_1 LQ at one-loop level [106]. Going beyond the leading-log approximation is necessary for the presence of vectorlike fermions, and it will also be a part of future work.

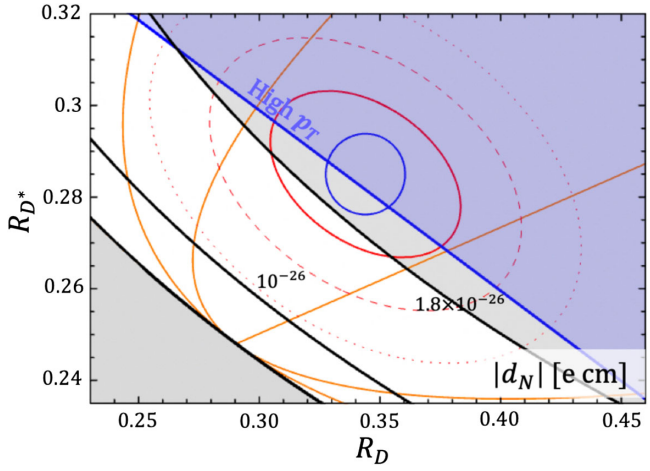

FIG. 7. Same as the Fig. 6, but the nucleon EDM is evaluated by the lattice charm tensor charge. The gray-shaded region in the upper right is excluded by the current upper bound on the neutron EDM [79].

ACKNOWLEDGMENTS

We thank Yohei Ema, Ulrich Nierste, Shohei Okawa, and Maxim Pospelov for their valuable comments and discussions. Furthermore, we would like to thank Hector Gisbert and Joan Ruiz Vidal for worthwhile discussions. We also appreciate Felix Wilsch for the technical support of HighPT. S. I. enjoys the support from the Deutsche Forschungsgemeinschaft (DFG, German Research Foundation) under Grant No. 396021762-TRR 257. S. I. would like to appreciate the "hot" hospitality at Universidad de Barcelona where the last stage of this project was made. T. K. was supported by the Grant-in-Aid for Scientific Research (C) from the Ministry of Education, Culture, Sports, Science, and Technology (MEXT), Japan, Grant No. 21K03572. This work is also supported by the Japan Society for the Promotion of Science (JSPS) Core-to-Core Program, Program No. JPJSCCA20200002.

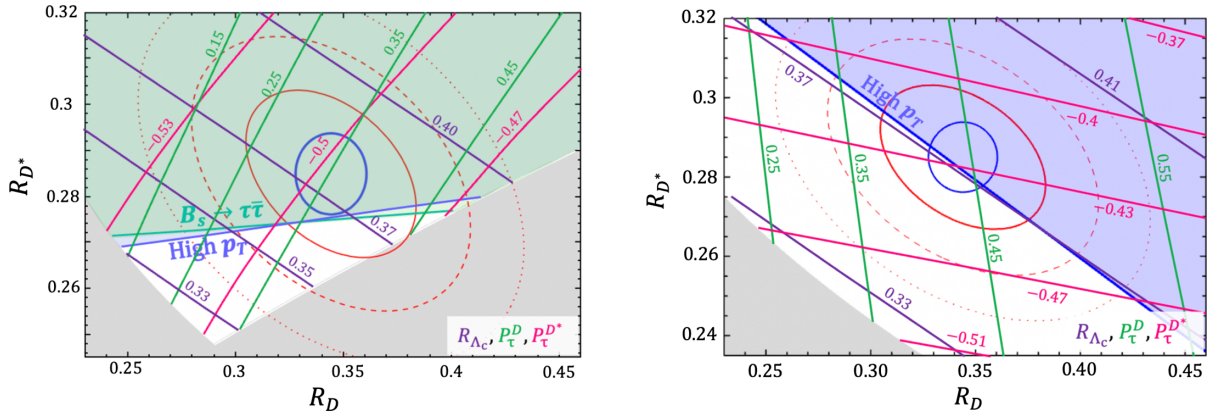

FIG. 8. Correlations with the τ polarization asymmetries, P_τ^D and $P_\tau^{D^*}$, and the LFU violation in $\Lambda_b \to \Lambda_c l\bar{\nu}$, R_{Λ_c}, are shown on the plane of R_D–R_{D^*} by the green, magenta, and purple contours, respectively, in the simplified U_1 (left panel) and R_2 LQ scenarios (right).

APPENDIX: OTHER $b \to c\tau\bar{\nu}$ OBSERVABLES

In this Appendix, other related observables in $b \to c\tau\bar{\nu}$ are discussed in the simplified U_1 LQ model and the R_2 LQ model. In Fig. 8, the τ polarization asymmetries in $\bar{B} \to D^{(*)}\tau\bar{\nu}$, P_τ^D and $P_\tau^{D^*}$ [113,114], and the LFU violation in $\Lambda_b \to \Lambda_c l\bar{\nu}$, $R_{\Lambda_c} \equiv \mathcal{B}(\Lambda_b \to \Lambda_c \tau\bar{\nu}_\tau)/\mathcal{B}(\Lambda_b \to \Lambda_c \ell\bar{\nu}_\ell)$, are shown by the green, magenta, and purple contours, respectively, for the simplified U_1 and R_2 LQ models.

In the U_1 LQ scenario, it is found that $P_\tau^{D^*}$ cannot deviate from the SM prediction $P_{\tau,\mathrm{SM}}^{D^*} \simeq -0.50$, while P_τ^D can deviate from $P_{\tau,\mathrm{SM}}^D \simeq 0.33$, which will be probed by the Belle II experiment with good accuracy [115]. On the other hand, a large value of R_{Λ_c} is expected compared to the SM prediction, $R_{\Lambda_c}^{\mathrm{SM}} \simeq 0.32$ [116]. This behavior is consistent with a sum rule prediction [117–119], and it should also be a smoking-gun signal in the LHCb experiment [120]. Note that the D^* longitudinal polarization ratio in $\bar{B} \to D^*\tau\bar{\nu}$, $F_L^{D^*}$ [113,121], is also predicted. It is, however, found that the U_1 LQ effect is tiny, $\Delta F_L^{D^*} = F_L^{D^*} - F_{L,\mathrm{SM}}^{D^*} = \pm 0.01$ [45,122], and it is smaller than the Belle II sensitivity [28].

In the R_2 LQ scenario, both P_τ^D and $P_\tau^{D^*}$ are expected to deviate from the SM predictions [21]. Also, the large value of R_{Λ_c} is expected in accordance with the sum rule. On the other hand, it is expected that $F_L^{D^*}$ cannot deviate: $\Delta F_L^{D^*} \simeq -0.01$ [45].

[1] *BABAR* Collaboration, Evidence for an excess of $\bar{B} \to D^{(*)}\tau^-\bar{\nu}_\tau$ decays, Phys. Rev. Lett. **109**, 101802 (2012).

[2] *BABAR* Collaboration, Measurement of an excess of $\bar{B} \to D^{(*)}\tau^-\bar{\nu}_\tau$ decays and implications for charged Higgs bosons, Phys. Rev. D **88**, 072012 (2013).

[3] Belle Collaboration, Measurement of the branching ratio of $\bar{B} \to D^{(*)}\tau^-\bar{\nu}_\tau$ relative to $\bar{B} \to D^{(*)}\ell^-\bar{\nu}_\ell$ decays with hadronic tagging at Belle, Phys. Rev. D **92**, 072014 (2015).

[4] Belle Collaboration, Measurement of the τ lepton polarization and $R(D^*)$ in the decay $\bar{B} \to D^*\tau^-\bar{\nu}_\tau$, Phys. Rev. Lett. **118**, 211801 (2017).

[5] Belle Collaboration, Measurement of the τ lepton polarization and $R(D^*)$ in the decay $\bar{B} \to D^*\tau^-\bar{\nu}_\tau$ with one-prong hadronic τ decays at Belle, Phys. Rev. D **97**, 012004 (2018).

[6] Belle Collaboration, Measurement of $\mathcal{R}(D)$ and $\mathcal{R}(D^*)$ with a semileptonic tagging method, arXiv:1904.08794.

[7] Belle Collaboration, Measurement of $\mathcal{R}(D)$ and $\mathcal{R}(D^*)$ with a semileptonic tagging method, Phys. Rev. Lett. **124**, 161803 (2020).

[8] LHCb Collaboration, Measurement of the ratio of branching fractions $\mathcal{B}(\bar{B}^0 \to D^{*+}\tau^-\bar{\nu}_\tau)/\mathcal{B}(\bar{B}^0 \to D^{*+}\mu^-\bar{\nu}_\mu)$, Phys. Rev. Lett. **115**, 111803 (2015); Phys. Rev. Lett. **115**, 159901(E) (2015).

[9] LHCb Collaboration, Measurement of the ratio of the $B^0 \to D^{*-}\tau^+\nu_\tau$ and $B^0 \to D^{*-}\mu^+\nu_\mu$ branching fractions using three-prong τ-lepton decays, Phys. Rev. Lett. **120**, 171802 (2018).

[10] LHCb Collaboration, Test of lepton flavor universality by the measurement of the $B^0 \to D^{*-}\tau^+\nu_\tau$ branching fraction using three-prong τ decays, Phys. Rev. D **97**, 072013 (2018).

[11] LHCb Collaboration, Measurement of the ratios of branching fractions $\mathcal{R}(D^*)$ and $\mathcal{R}(D^0)$, Phys. Rev. Lett. **131**, 111802 (2023).

[12] LHCb Collaboration, Test of lepton flavour universality using $B^0 \to D^{*-}\tau^+\nu_\tau$ decays with hadronic τ channels,

Phys. Rev. D **108**, 012018 (2023); Phys. Rev. D **109**, 119902(E) (2024).
[13] Belle II Collaboration, Recent Belle II results on semileptonic B decays and tests of lepton-flavor universality, https://indico.cern.ch/event/1114856/contributions/5423684/.
[14] Belle-II Collaboration, A test of lepton flavor universality with a measurement of $R(D^*)$ using hadronic B tagging at the Belle II experiment, arXiv:2401.02840.
[15] LHCb Collaboration, $b \to c l \nu$ decays at LHCb, https://indico.in2p3.fr/event/32664/timetable/?view=standard_numbered#38-b-to-c-l-nu-decays-at-lhcb.
[16] Heavy Flavor Averaging Group, HFLAV Collaboration, Averages of b-hadron, c-hadron, and τ-lepton properties as of 2021, Phys. Rev. D **107**, 052008 (2023).
[17] HFLAV Collaboration, "Preliminary average of $R(D)$ and $R(D^*)$ for Moriond 2024" at https://hflav-eos.web.cern.ch/hflav-eos/semi/moriond24/html/RDsDsstar/RDRDs.html.
[18] M. Bordone, N. Gubernari, D. van Dyk, and M. Jung, Heavy-Quark expansion for $\bar{B}_s \to D_s^{(*)}$ form factors and unitarity bounds beyond the $SU(3)_F$ limit, Eur. Phys. J. C **80**, 347 (2020).
[19] S. Iguro and R. Watanabe, Bayesian fit analysis to full distribution data of $\bar{B} \to D^{(*)} \ell \bar{\nu}$: $|V_{cb}|$ determination and new physics constraints, J. High Energy Phys. 08 (2020) 006.
[20] F. U. Bernlochner *et al.*, Constrained second-order power corrections in HQET: $R(D^{(*)})$, $|V_{cb}|$, and new physics, Phys. Rev. D **106**, 096015 (2022).
[21] S. Iguro, T. Kitahara, and R. Watanabe, Global fit to $b \to c\tau\nu$ anomalies as of Spring 2024, arXiv:2405.06062.
[22] D. London and J. Matias, B flavour anomalies: 2021 Theoretical status report, Annu. Rev. Nucl. Part. Sci. **72**, 37 (2022).
[23] L. Di Luzio, A. Greljo, and M. Nardecchia, Gauge leptoquark as the origin of B-physics anomalies, Phys. Rev. D **96**, 115011 (2017).
[24] M. Bordone, C. Cornella, J. Fuentes-Martin, and G. Isidori, A three-site gauge model for flavor hierarchies and flavor anomalies, Phys. Lett. B **779**, 317 (2018).
[25] M. Bordone, C. Cornella, J. Fuentes-Martín, and G. Isidori, Low-energy signatures of the PS^3 model: From B-physics anomalies to LFV, J. High Energy Phys. 10 (2018) 148.
[26] L. Calibbi, A. Crivellin, and T. Li, Model of vector leptoquarks in view of the B-physics anomalies, Phys. Rev. D **98**, 115002 (2018).
[27] B. Capdevila, A. Crivellin, S. Descotes-Genon, L. Hofer, and J. Matias, Searching for new physics with $b \to s\tau^+\tau^-$ processes, Phys. Rev. Lett. **120**, 181802 (2018).
[28] Belle-II Collaboration, The Belle II physics book, Prog. Theor. Exp. Phys. **2019**, 123C01 (2019); Prog. Theor. Exp. Phys. **2020**, 029201(E) (2020).
[29] A. Cerri *et al.*, Report from Working Group 4: Opportunities in flavour physics at the HL-LHC and HE-LHC, CERN Yellow Rep. Monogr. **7**, 867 (2019).
[30] P. Q. Hung, A. J. Buras, and J. D. Bjorken, Petite unification of quarks and leptons, Phys. Rev. D **25**, 805 (1982).
[31] G. Valencia and S. Willenbrock, Quark—lepton unification and rare meson decays, Phys. Rev. D **50**, 6843 (1994).
[32] A. Pomarol and D. Tommasini, Horizontal symmetries for the supersymmetric flavor problem, Nucl. Phys. **B466**, 3 (1996).
[33] R. Barbieri, G. R. Dvali, and L. J. Hall, Predictions from a U(2) flavor symmetry in supersymmetric theories, Phys. Lett. B **377**, 76 (1996).
[34] R. Barbieri, G. Isidori, J. Jones-Perez, P. Lodone, and D. M. Straub, $U(2)$ and minimal flavour violation in supersymmetry, Eur. Phys. J. C **71**, 1725 (2011).
[35] R. Barbieri, G. Isidori, A. Pattori, and F. Senia, Anomalies in B-decays and $U(2)$ flavour symmetry, Eur. Phys. J. C **76**, 67 (2016).
[36] G. Panico, A. Pomarol, and M. Riembau, EFT approach to the electron electric dipole moment at the two-loop level, J. High Energy Phys. 04 (2019) 090.
[37] W. Altmannshofer, S. Gori, H. H. Patel, S. Profumo, and D. Tuckler, Electric dipole moments in a leptoquark scenario for the B-physics anomalies, J. High Energy Phys. 05 (2020) 069.
[38] W. Dekens, J. de Vries, M. Jung, and K. K. Vos, The phenomenology of electric dipole moments in models of scalar leptoquarks, J. High Energy Phys. 01 (2019) 069.
[39] H. Gisbert and J. Ruiz Vidal, Improved bounds on heavy quark electric dipole moments, Phys. Rev. D **101**, 115010 (2020).
[40] K. S. Babu, P. S. B. Dev, S. Jana, and A. Thapa, Unified framework for B-anomalies, muon $g-2$ and neutrino masses, J. High Energy Phys. 03 (2021) 179.
[41] D. Bečirević *et al.*, Model with two scalar leptoquarks: R2 and S3, Phys. Rev. D **106**, 075023 (2022).
[42] M. Kirk, S. Okawa, and K. Wu, A ν window onto leptoquarks?, J. High Energy Phys. 12 (2023) 093.
[43] C. Cornella, J. Fuentes-Martin, and G. Isidori, Revisiting the vector leptoquark explanation of the B-physics anomalies, J. High Energy Phys. 07 (2019) 168.
[44] M. J. Baker, J. Fuentes-Martín, G. Isidori, and M. König, High- p_T signatures in vector–leptoquark models, Eur. Phys. J. C **79**, 334 (2019).
[45] S. Iguro, T. Kitahara, Y. Omura, R. Watanabe, and K. Yamamoto, D* polarization vs. $R_{D^{(*)}}$ anomalies in the leptoquark models, J. High Energy Phys. 02 (2019) 194.
[46] F. S. Queiroz and W. Shepherd, New physics contributions to the muon anomalous magnetic moment: A numerical code, Phys. Rev. D **89**, 095024 (2014).
[47] K. Kowalska, E. M. Sessolo, and Y. Yamamoto, Constraints on charmphilic solutions to the muon g-2 with leptoquarks, Phys. Rev. D **99**, 055007 (2019).
[48] W. Dekens and J. de Vries, Renormalization group running of dimension-six sources of parity and time-reversal violation, J. High Energy Phys. 05 (2013) 149.
[49] E. E. Jenkins, A. V. Manohar, and P. Stoffer, Low-energy effective field theory below the electroweak scale: Anomalous dimensions, J. High Energy Phys. 01 (2018) 084.
[50] G. Degrassi, E. Franco, S. Marchetti, and L. Silvestrini, QCD corrections to the electric dipole moment of the neutron in the MSSM, J. High Energy Phys. 11 (2005) 044.

[51] A. Crivellin and F. Saturnino, Correlating tauonic B decays with the neutron electric dipole moment via a scalar leptoquark, Phys. Rev. D **100**, 115014 (2019).
[52] U. Haisch and G. Koole, Beautiful and charming chromodipole moments, J. High Energy Phys. 09 (2021) 133.
[53] A. G. Grozin, I. B. Khriplovich, and A. S. Rudenko, Electric dipole moments from e to tau, Phys. Atom. Nucl. **72**, 1203 (2009).
[54] Y. Ema, T. Gao, and M. Pospelov, Improved indirect limits on muon electric dipole moment, Phys. Rev. Lett. **128**, 131803 (2022).
[55] Y. Ema, T. Gao, and M. Pospelov, Improved indirect limits on charm and bottom quark EDMs, J. High Energy Phys. 07 (2022) 106.
[56] M. Pospelov and A. Ritz, CKM benchmarks for electron electric dipole moment experiments, Phys. Rev. D **89**, 056006 (2014).
[57] K. Kaneta, N. Nagata, K. A. Olive, M. Pospelov, and L. Velasco-Sevilla, Quantifying limits on CP violating phases from EDMs in supersymmetry, J. High Energy Phys. 03 (2023) 250.
[58] Y. Ema, T. Gao, and M. Pospelov, Reevaluation of heavy-fermion-induced electron EDM at three loops, Phys. Lett. B **835**, 137496 (2022).
[59] T. S. Roussy *et al.*, A new bound on the electron's electric dipole moment, Science **381**, 46 (2023).
[60] G. Boyd, A. K. Gupta, S. P. Trivedi, and M. B. Wise, Effective Hamiltonian for the electric dipole moment of the neutron, Phys. Lett. B **241**, 584 (1990).
[61] E. Braaten, C.-S. Li, and T.-C. Yuan, The evolution of Weinberg's gluonic CP violation operator, Phys. Rev. Lett. **64**, 1709 (1990).
[62] D. Chang, W.-Y. Keung, C. S. Li, and T. C. Yuan, QCD corrections to CP violation from color electric dipole moment of b quark, Phys. Lett. B **241**, 589 (1990).
[63] M. Pospelov and A. Ritz, Neutron EDM from electric and chromoelectric dipole moments of quarks, Phys. Rev. D **63**, 073015 (2001).
[64] M. Pospelov and A. Ritz, Electric dipole moments as probes of new physics, Ann. Phys. (Amsterdam) **318**, 119 (2005).
[65] J. Hisano, J. Y. Lee, N. Nagata, and Y. Shimizu, Reevaluation of neutron electric dipole moment with QCD sum rules, Phys. Rev. D **85**, 114044 (2012).
[66] K. Fuyuto, J. Hisano, N. Nagata, and K. Tsumura, QCD corrections to quark (chromo)electric dipole moments in high-scale supersymmetry, J. High Energy Phys. 12 (2013) 010.
[67] C. Alexandrou *et al.*, Nucleon axial, tensor, and scalar charges and σ-terms in lattice QCD, Phys. Rev. D **102**, 054517 (2020).
[68] D. A. Demir, M. Pospelov, and A. Ritz, Hadronic EDMs, the Weinberg operator, and light gluinos, Phys. Rev. D **67**, 015007 (2003).
[69] U. Haisch and A. Hala, Sum rules for CP-violating operators of Weinberg type, J. High Energy Phys. 11 (2019) 154.
[70] N. Yamanaka and E. Hiyama, Weinberg operator contribution to the nucleon electric dipole moment in the quark model, Phys. Rev. D **103**, 035023 (2021).
[71] T. Bhattacharya, V. Cirigliano, R. Gupta, and B. Yoon, Quark chromoelectric dipole moment contribution to the neutron electric dipole moment, *Proc. Sci.*, LATTICE2016 (2016) 225 [arXiv:1612.08438].
[72] B. Yoon, T. Bhattacharya, and R. Gupta, Neutron electric dipole moment on the lattice, EPJ Web Conf. **175**, 01014 (2018).
[73] E. Mereghetti, Lattice QCD and nuclear physics for searches of physics beyond the standard model, *Proc. Sci.*, LATTICE2018 (2019) 002 [arXiv:1812.11238].
[74] B. Yoon, T. Bhattacharya, V. Cirigliano, and R. Gupta, Neutron electric dipole moments with clover fermions, *Proc. Sci.*, LATTICE2019 (2020) 243 [arXiv:2003.05390].
[75] A. Todaro, C. Alexandrou, A. Athenodorou, and K. Hadjiannakou, A lattice QCD determination of the neutron electric dipole moment at the physical point, *Proc. Sci.*, LATTICE2021 (2022) 120 [arXiv:2112.03989].
[76] T. Bhattacharya, V. Cirigliano, R. Gupta, E. Mereghetti, and B. Yoon, Calculation of neutron electric dipole moment due to the QCD topological term, Weinberg three-gluon operator and the quark chromoelectric moment, *Proc. Sci.*, LATTICE2021 (2022) 567 [arXiv:2203.03746].
[77] T. Bhattacharya, V. Cirigliano, R. Gupta, E. Mereghetti, and B. Yoon, nEDM from the theta-term and chromoEDM operators, *Proc. Sci.*, LATTICE2022 (2023) 304 [arXiv:2301.08161].
[78] R. Alarcon *et al.*, Snowmass 2021, arXiv:2203.08103.
[79] C. Abel *et al.*, Measurement of the permanent electric dipole moment of the neutron, Phys. Rev. Lett. **124**, 081803 (2020).
[80] n2EDM Collaboration, The design of the n2EDM experiment: nEDM Collaboration, Eur. Phys. J. C **81**, 512 (2021).
[81] J. W. Martin, Current status of neutron electric dipole moment experiments, J. Phys. Conf. Ser. **1643**, 012002 (2020).
[82] T. M. Ito *et al.*, Performance of the upgraded ultracold neutron source at Los Alamos National Laboratory and its implication for a possible neutron electric dipole moment experiment, Phys. Rev. C **97**, 012501(R) (2018).
[83] D. Wurm *et al.*, The PanEDM neutron electric dipole moment experiment at the ILL, EPJ Web Conf. **219**, 02006 (2019).
[84] nEDM Collaboration, A new cryogenic apparatus to search for the neutron electric dipole moment, J. Instrum. **14**, P11017 (2019).
[85] B. K. Sahoo, Improved limits on the hadronic and semi-hadronic CP violating parameters and role of a dark force carrier in the electric dipole moment of ^{199}Hg, Phys. Rev. D **95**, 013002 (2017).
[86] CPEDM Collaboration, *Storage Ring to Search for Electricdipole Moments of Charged Particles: Feasibility Study* (CERN, Geneva, 2021).
[87] J. Alexander *et al.*, The storage ring proton EDM experiment, arXiv:2205.00830.
[88] J. Aebischer, M. Fael, C. Greub, and J. Virto, B physics beyond the standard model at one loop: Complete renormalization group evolution below the electroweak scale, J. High Energy Phys. 09 (2017) 158.

[89] M. González-Alonso, J. Martin Camalich, and K. Mimouni, Renormalization-group evolution of new physics contributions to (semi)leptonic meson decays, Phys. Lett. B **772**, 777 (2017).
[90] J. Aebischer, A. Crivellin, and C. Greub, QCD improved matching for semileptonic B decays with leptoquarks, Phys. Rev. D **99**, 055002 (2019).
[91] LHCb Collaboration, Search for the decays $B_s^0 \to \tau^+\tau^-$ and $B^0 \to \tau^+\tau^-$, Phys. Rev. Lett. **118**, 251802 (2017).
[92] LHCb Collaboration, Physics case for an LHCb Upgrade II—Opportunities in flavour physics, and beyond, in the HL-LHC era, arXiv:1808.08865.
[93] L. Allwicher, D. A. Faroughy, F. Jaffredo, O. Sumensari, and F. Wilsch, HighPT: A tool for high-pT Drell-Yan tails beyond the standard model, Comput. Phys. Commun. **289**, 108749 (2023).
[94] ATLAS Collaboration, Search for heavy Higgs bosons decaying into two tau leptons with the ATLAS detector using pp collisions at $\sqrt{s} = 13$ TeV, Phys. Rev. Lett. **125**, 051801 (2020).
[95] A. Bhaskar, D. Das, T. Mandal, S. Mitra, and C. Neeraj, Precise limits on the charge-2/3 U1 vector leptoquark, Phys. Rev. D **104**, 035016 (2021).
[96] CMS Collaboration, The search for a third-generation leptoquark coupling to a τ lepton and a b quark through single, pair and nonresonant production at $\sqrt{s} = 13$ TeV, https://cds.cern.ch/record/2815309.
[97] CMS Collaboration, Searches for additional Higgs bosons and for vector leptoquarks in $\tau\tau$ final states in proton-proton collisions at $\sqrt{s} = 13$ TeV, J. High Energy Phys. 07 (2023) 073.
[98] CMS Collaboration, A flavor for leptoquarks, https://indico.cern.ch/event/1114856/contributions/5360087/.
[99] A. Greljo, J. Martin Camalich, and J. D. Ruiz-Álvarez, Mono-τ signatures at the LHC constrain explanations of B-decay anomalies, Phys. Rev. Lett. **122**, 131803 (2019).
[100] S. Iguro, M. Takeuchi, and R. Watanabe, Testing leptoquark/EFT in $\bar{B} \to D^{(*)} l\bar{\nu}$ at the LHC, Eur. Phys. J. C **81**, 406 (2021).
[101] D. Marzocca, U. Min, and M. Son, Bottom-flavored mono-tau tails at the LHC, J. High Energy Phys. 12 (2020) 035.
[102] M. Endo, S. Iguro, T. Kitahara, M. Takeuchi, and R. Watanabe, Non-resonant new physics search at the LHC for the b → c$\tau\nu$ anomalies, J. High Energy Phys. 02 (2022) 106.
[103] L. Di Luzio, J. Fuentes-Martin, A. Greljo, M. Nardecchia, and S. Renner, Maximal flavour violation: A Cabibbo mechanism for leptoquarks, J. High Energy Phys. 11 (2018) 081.
[104] J. Fuentes-Martín, G. Isidori, M. König, and N. Selimović, Vector leptoquarks beyond tree level III: Vector-like fermions and flavor-changing transitions, Phys. Rev. D **102**, 115015 (2020).
[105] D. Marzocca, Addressing the B-physics anomalies in a fundamental composite Higgs model, J. High Energy Phys. 07 (2018) 121.
[106] A. Crivellin, C. Greub, D. Müller, and F. Saturnino, Importance of loop effects in explaining the accumulated evidence for new physics in B decays with a vector leptoquark, Phys. Rev. Lett. **122**, 011805 (2019).
[107] S. Iguro, J. Kawamura, S. Okawa, and Y. Omura, Importance of vector leptoquark-scalar box diagrams in Pati-Salam unification with vector-like families, J. High Energy Phys. 07 (2022) 022.
[108] V. Cirigliano, W. Dekens, J. de Vries, and E. Mereghetti, Is there room for CP violation in the top-Higgs sector?, Phys. Rev. D **94**, 016002 (2016).
[109] K. Fuyuto, M. Ramsey-Musolf, and T. Shen, Electric dipole moments from CP-violating scalar leptoquark interactions, Phys. Lett. B **788**, 52 (2019).
[110] J. Hisano, K. Tsumura, and M. J. S. Yang, QCD corrections to neutron electric dipole moment from dimension-six four-quark operators, Phys. Lett. B **713**, 473 (2012).
[111] P. Arnan, D. Becirevic, F. Mescia, and O. Sumensari, Probing low energy scalar leptoquarks by the leptonic W and Z couplings, J. High Energy Phys. 02 (2019) 109.
[112] A. Crivellin, C. Greub, D. Müller, and F. Saturnino, Scalar leptoquarks in leptonic processes, J. High Energy Phys. 02 (2021) 182.
[113] M. Tanaka and R. Watanabe, New physics in the weak interaction of $\bar{B} \to D^{(*)}\tau\bar{\nu}$, Phys. Rev. D **87**, 034028 (2013).
[114] P. Asadi, M. R. Buckley, and D. Shih, Asymmetry observables and the origin of $R_{D^{(*)}}$ anomalies, Phys. Rev. D **99**, 035015 (2019).
[115] R. Alonso, J. Martin Camalich, and S. Westhoff, Tau properties in $B \to D\tau\nu$ from visible final-state kinematics, Phys. Rev. D **95**, 093006 (2017).
[116] F. U. Bernlochner, Z. Ligeti, D. J. Robinson, and W. L. Sutcliffe, New predictions for $\Lambda_b \to \Lambda_c$ semileptonic decays and tests of heavy quark symmetry, Phys. Rev. Lett. **121**, 202001 (2018).
[117] M. Blanke *et al.*, Impact of polarization observables and $B_c \to \tau\nu$ on new physics explanations of the $b \to c\tau\nu$ anomaly, Phys. Rev. D **99**, 075006 (2019).
[118] M. Blanke *et al.*, Addendum to "Impact of polarization observables and $B_c \to \tau\nu$ on new physics explanations of the $b \to c\tau\nu$ anomaly", Phys. Rev. D **100**, 035035 (2019).
[119] M. Fedele *et al.*, Impact of Λb → Λc$\tau\nu$ measurement on new physics in b → clν transitions, Phys. Rev. D **107**, 055005 (2023).
[120] LHCb Collaboration, Observation of the decay $\Lambda_b^0 \to \Lambda_c^+\tau^-\bar{\nu}_\tau$, Phys. Rev. Lett. **128**, 191803 (2022).
[121] Belle Collaboration in *10th International Workshop on the CKM Unitarity Triangle* (2019), arXiv:1903.03102.
[122] J. Fuentes-Martín, G. Isidori, J. Pagès, and K. Yamamoto, With or without U(2)? Probing non-standard flavor and helicity structures in semileptonic B decays, Phys. Lett. B **800**, 135080 (2020).